Article

Spatially-Resolved Ultrafast Optical Spectroscopy of Polymer-Grafted Residues on CVD Graphene

Guannan Yu,[†] Xinfeng Liu,[†] Guichuan Xing,[†,2,3] Shi Chen,[†] Chin Fan Ng,[†] Xiangyang Wu,[‖] Edwin Kok Lee Yeow,[‖] Wen Siang Lew,[†] and Tze Chien Sum*[,†,2,3]

[†]Division of Physics and Applied Physics and [‖]Division of Chemistry and Biological Chemistry, School of Physical and Mathematical Sciences, Nanyang Technological University, 21 Nanyang Link, Singapore 637371

[2]Energy Research Institute @ NTU (ERI@N), Nanyang Technological University, 50 Nanyang Drive, Singapore 637553

[3]Singapore-Berkeley Research Initiative for Sustainable Energy (SinBeRISE), 1 Create Way, Singapore 138602

S *Supporting Information*

ABSTRACT: A recent report proved that polymer residues become grafted to graphene despite the efforts to clean the surface by thermal annealing [Lin, Y.-C., et al. *Nano Lett.* **2012**, *12*, 414]. Such residues inevitably originate from the photoresist (e.g., poly(methyl methacrylate) (PMMA)) used for graphene transfer and device processing. Here, through spatially resolved transient absorption spectroscopy and transient photoluminescence spectroscopy, we investigate the effects of such polymer-grafted residues on the carrier dynamics of CVD graphene. The presence of these polymer-grafted residues is validated by both X-ray photoelectron spectroscopy and micro-Raman spectroscopy. Unlike the ultrafast nonradiative recombination at the pristine graphene, these regions exhibit distinct long-lived carrier dynamics that undergo radiative recombination, which is characteristic of the opening of the graphene bandgap. Understanding the influence of such defects on the carrier dynamics and relaxation pathways is key to modifying the optoelectronic properties of graphene-based devices.
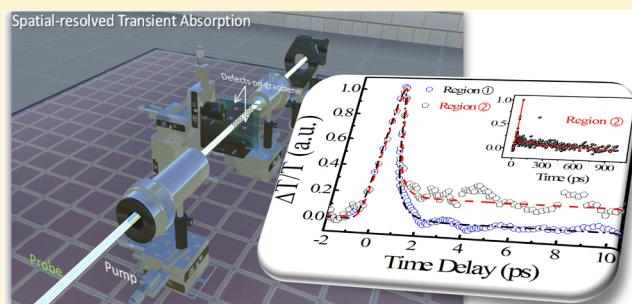
INTRODUCTION

Graphene is a new class of nanomaterials comprising a single two-dimensional atomic layer of carbon atoms arranged in a hexagonal lattice.[1] Graphene's unique band structure endows it with a linear dispersion relationship near the K point of the Brillion zone. This gives rise to its exceptional properties of high electronic velocity ($\sim 10^6$ m/s) and mobility (~ 15000 cm^2/ (Vs)), that are particularly attractive for optoelectronic applications.[2,3] This novel material has attracted substantial research efforts for applications ranging from nanoscale optoelectronic devices,[4,5] single layer transistors, biosensors, and energy storage devices. The key to optimizing and tailoring graphene's optoelectronic properties for practical applications is through a clear understanding of its carrier interactions and recombination dynamics. Although there are extensive studies on the carrier dynamics and relaxation mechanisms in high quality, pristine graphene lattices,[6−10] reports focusing on the influence of defects on the carrier dynamics in graphene are few and far between. In particular, there are no reports on the effects of grafted polymer residues on the carrier dynamics in graphene.

Presently, the established method for transferring a large area graphene sheet involves the use of poly(methyl methacrylate) (PMMA) as a temporary support film during the etching of

metal foil to prevent folding and rippling of the graphene sheet.[11,12] Annealing is then employed for the removal of the residual PMMA, but a recent report casts doubts on the cleanliness of the resultant graphene surface.[13] In that work, high-resolution transmission electron microscopy revealed that the polymer residues remain on the graphene despite the annealing efforts. The reconstruction of the carbon atoms from sp^2 to sp^3 at these locations has a pronounced impact on the intrinsic properties of graphene. From the standpoint of fundamental scientific interest and for practical applications, it is therefore imperative to gain a deep insight into the influence of such residual polymer-induced defects on the carrier dynamics and relaxation pathways. Elucidating the dynamical carrier interaction signatures and the relaxation mechanisms at these defect sites is the main focus of this paper.

Herein, spatially resolved transient optical spectroscopies (i.e., transient absorption spectroscopy (TAS) and time-resolved photoluminescence (TRPL)) were employed to investigate the effects of residual polymer-induced defects in CVD graphene on the ultrafast carrier dynamics. Spatially

resolved transient optical spectroscopy[14−17] provides research- ers with a powerful characterization tool to investigate the carrier dynamics of such defects in their locality. We wish to emphasize that the spatially resolved transient optical spectros- copy performed on the order of several micrometers is still very much an ensemble average. Nevertheless, in the time domain, these techniques are extremely sensitive to the presence of the defects on graphene sheet, which manifest in the ensuing carrier dynamics. The presence of such residuals is verified using complementary techniques of X-ray photoelectron spectrosco- py (XPS) and micro-Raman spectroscopy. Our findings revealed the presence of an additional long decay lifetime at these defect sites—attributed to the opening of the graphene bandgap as a consequence of the grafting of the polymer molecules. Our work provides clear experimental evidence of modulated fast electron−hole recombination dynamics in graphene by residual polymer-grafted defects. Potentially, this simple approach of modulating the electronic band structure of graphene with organic residuals may find practical use in tailoring the optoelectronic properties of graphene for light harvesting and spin manipulation, and so forth.

■ EXPERIMENTAL SECTION

CVD Graphene Samples. Commercial samples of single layer graphene thin films (as-grown on Cu foils and transferred on quartz) were purchased from Graphene Supermarket. Briefly, their fabrication is based on a low pressure chemical vapor deposition method reported before[18] on a flat Cu foil in a three-zone vacuum (10^{-3} Torr) furnace at temperatures of 950−1050 °C.

Substrate Transfer. Single layer graphene thin film was transferred to a quartz substrate using the PMMA coating technique.[11] After this wet etching process, the transferred graphene was annealed at 250 °C in an Ar atmosphere for 2 h. Typically, samples with low defect density have been obtained using this transfer process. Based on this transfer method, Lin et al. proposed a mechanism for the chain scission and grafting of the macroradicals with graphene defect sites that leads to the rehybridization of carbon from sp^2 to sp^3.[13]

Characterization of the Transferred CVD Graphene Thin Film. XPS measurements were performed using a VG ESCALAB 220i-XL system with a monochromatic Al K_α (1486.6 eV) X-ray source. Micro-Raman measurements were performed using a LabRAM HR (Horiba) Raman microscope system.

Spatially Resolved Optical Spectroscopy. Fluorescence lifetime imaging microscopy (FLIM) was performed using a time-resolved confocal microscope (MicroTime 200, Pico- Quant). A 405 nm pulsed laser (pulse width <300 ps) with repetition rate of ∼20 MHz and energy ∼0.15 μW was used to excite the samples and the fluorescence was detected by a single-photon avalanche diode (SPAD, SPCM-AQR-15, Perkin- Elmer) after passing through an emission filter (HQ 430 LP, Chroma). Spatially resolved femtosecond TAS was performed using a home-built pump−probe setup equipped with micro- scope objectives (see Supporting Information for schematic S1). Frequency doubled pulses (400 nm) from a 1 kHz regenerative amplifier (150 fs) were used as the pump, while the probe comprises a weaker fundamental 800 nm pulse. Both the pump and probe beam were overlapped and aligned coaxially to pass through a 100× objective lens (N.A. 0.7), slightly defocused to a ∼5−10 μm spot. After passing through the sample, the pump beam was subsequently filtered by a 495

nm long pass filter, while the probe beam was collected by a 50× objective lens (N.A. 0.55) to a silicon photodetector. Pump-induced changes of transmission ($\Delta T/T$) of the probe beam were monitored using a monochromator/photomultiplier tube (PMT) configuration with lock-in detection. The pump beam was chopped at 83 Hz and this was used as the reference frequency for the lock-in amplifier. The pump fluence was kept below 20 μJ/cm^2 per pulse in order to avoid any photodamage to the samples.[19]

■ RESULTS AND DISCUSSION

The presence of residual polymer grafting in pristine graphene lattice was experimentally verified using XPS. Figure 1a shows a
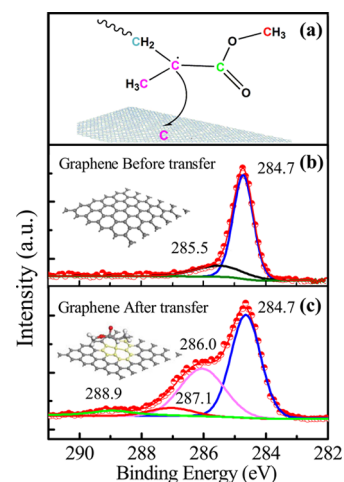

Figure 1. (a) Schematic of a PMMA macroradical grafting onto a pristine sheet of graphene. (b) XPS spectra of monolayer CVD graphene thin film on Cu foil before the transfer. (c) XPS spectra of monolayer CVD graphene thin film on quartz substrate after the transfer. Inset of (b) and (c) gives an illustration of the surface of the graphene sample.

schematic of a typical macroradical following the scission of PMMA. Figure 1b,c shows the XPS spectra of a single layer graphene thin film before and after transfer, respectively. The main peak in Figure 1b (284.7 eV − red line) arises from carbon sp^2 hybridization in pristine graphene.[20] Following the transfer, several new peaks appear in Figure 1c due to the presence of the polymer residues. From the analysis of peak fitting, the main peak (284.7 and 286.0 eV − black and pink peak) in Figure 1c originates from the rehybridization of the carbon−carbon sp^2 and sp^3 bonds arising from the grafting of the polymer residues with graphene. Within these peaks, the 286.0 eV peak comes from carbon−carbon bonds in PMMA (see Supporting Information S2). The presence of two other peaks (located at 287.1 and 288.9 eV) in Figure 1c provides further validation of the grafting of the polymer residues to graphene. They arise from the carbon−oxygen single bond (C−O) and the carboxylic group in the macroradicals, respectively. The ratio of their peak intensity is approximately 1:1, which is consistent with the chemical composition of the macroradical (Figure 1 a).

Next, micro-Raman measurements were performed to establish the location of the defects on the graphene sample (on quartz). Figure 2 (inset) shows a representative micro- Raman map (based on D peak 1324 cm^{-1}) of a typical polymer-grafted-graphene region. As the distribution of the
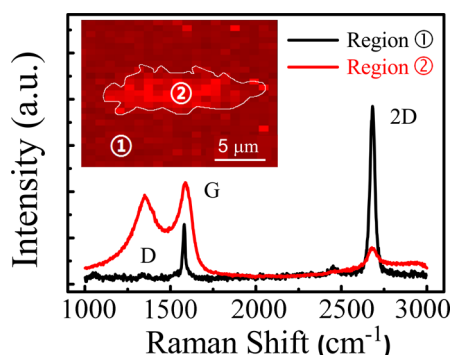
Figure 2. Raman characterization of a region of pristine graphene (Region ①) and a region with residual polymer (Region ②). Inset shows the Raman map of the D peak (1350 cm^{-1}) of this 30 μm × 30 μm region where ① and ② give the approximate location where the Raman spectra are extracted.

polymer residues is not uniform on the graphene sheet, we had selected region ① that is relatively defect-free and region ② with the polymer residue present. The Raman spectra at both regions are overlaid for comparison. In region ①, the Raman profile is characteristic of typical monolayer graphene lattice with a sharp G peak (1581 cm^{-1}) and 2D peak (2708 cm^{-1}). The low-intensity D peak (1324 cm^{-1}) indicates a complete sp^2 lattice structure. The absence of any PMMA-related peaks (typically located at 1460 cm^{-1} and 1648 cm^{-1} following 632 nm excitation[13,21]) indicates that there is no residual PMMA in region ①. On the other hand, the Raman profile in region ② shows a more pronounced D peak that is typically associated with the presence of defects.[22−24] In addition, the I_{2D}/I_G ratio is also reduced which is characteristic of doping in graphene.[25,26] The graphene D and G peaks are broadened due to the presence of overlapping contributions from the PMMA peaks.

FLIM maps in Figure 3a−e show a weak photoluminescence (PL) emission from the polymer grafted region (with an excitation power of ∼0.15 μW). The PL signatures on the same sample location over the various spectral regions were collected using a set of long pass filters. A spectrometer was not used to disperse the emission as the losses from the gratings were too significant. Control experiments were also performed to
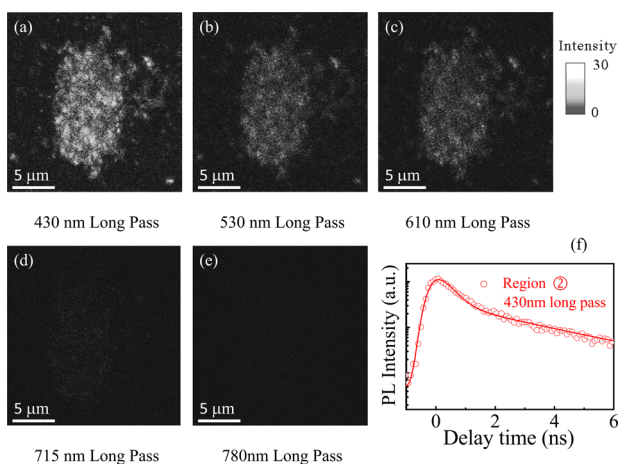

Figure 3. (a)−(e) FLIM images of region ② collected with different long pass filters. These images indicate the presence of a broad emission peak. (f) Transient PL decay from region ② collected with a 430 nm long pass filter.

eliminate any possibility that the emission is from the quartz slide, PMMA film, and any interaction between the deposited PMMA film and graphene (no annealing)—see Supporting Information S3. The PL emission is uniformly distributed over the polymer residue (region ②). As for the regions of pristine graphene (i.e., the dark parts around the polymer residue—region ①), no emission is observed as expected from its conical band structure. The PL emission from region ② becomes weaker as the filter cutoff wavelength becomes redder. This shows that polymer residue gives a broad PL emission spanning from the visible range to NIR. DFT calculations of the MMA–graphene complexes with local density approximations revealed that the polymer-grafted defects modify the band structure near the Fermi level and significantly reduce the Femi velocity.[13] Furthermore, an energy gap appears due to the local rehybridization of carbon atoms from sp^2 to sp^3. Observations of such PL emission from Region ② strongly suggest the opening of the bandgap and the introduction of localized states in pristine graphene. Strictly, there are important differences in the details of the electronic structure modification through the grafting of the polymer residue in CVD graphene sheet and the insertion of the oxygen functional group in GO,[27] but the common effects of bandgap opening and the presence of localized states would nonetheless affect the carrier dynamics in a similar and consistent manner.

The PL dynamics (as shown in Figure 3f) are well-fitted with a biexponential decay function with lifetime components τ_1 (∼265 ps) and τ_2 (∼2.89 ns). The shorter lifetime τ_1 is attributed to arise from electron−hole (e−h) recombination between the localized states in the conduction band (CB) with those in the valence band (VB), while the longer ns lifetime is attributed to e−h recombination from the bottom of the CB to states in the VB. This assignment is consistent with the findings from graphene oxide (an equivalent system with a bandgap).[13] Further validation of this recombination mechanism can be obtained from TAS.

Figure 4 shows the differential transmittance (DT) transients at regions ① and ② that are fitted using a monoexponential and
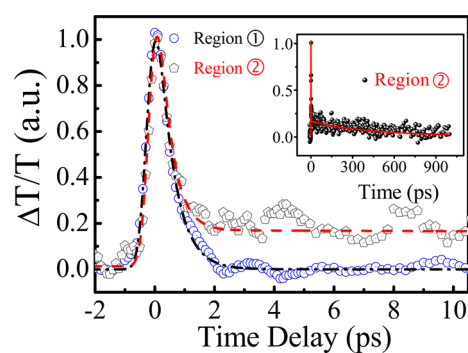

Figure 4. Spatially resolved DT transients of Region ① (blue circles) and Region ② (black pentagons) following 400 nm pump/800 nm probe at a pump fluence of ∼11 μJ/cm^2. Inset shows the DT transient of Region ② over a longer delay time of 1 ns.

biexponential function, respectively. Both regions exhibit photobleaching (PB) signatures (i.e., $\Delta T/T > 0$) with a rapid rise in $\Delta T/T$ due to state-filling and is followed by the recovery of DT profile to equilibrium through relaxation processes. In fact, there is also a very long-lived few nanoseconds lifetime component in region ② that is only evident on a longer time scale (see Figure 4 inset). Due to the limitations of our micro-

TA setup, the relaxation dynamics of the electron and phonon interactions within the first few hundred femtoseconds of the PB signature in region ① are convolved (i.e., $\tau'_1 = 0.5 \pm 0.1$ ps − see Table 1). Control experiments involving PMMA only

Table 1. TA Lifetimes of Region① (Pristine Graphene) and Region② (Polymer Grafted Graphene) Following 400 nm Pump/800 nm Probe[a]

	short lifetime component (ps)	A_1 (%)	long lifetime component (ps)	A_2 (%)
Region ①	$\tau'_1 = 0.5 \pm 0.1$	-	-	-
Region ②	$\tau''_1 = 0.4 \pm 0.1$	94	$\tau''_2 = 390 \pm 50$	6

[a]Pump fluence is ~11 μJ/cm^2.

films yielded null DT signals, while those involving PMMA films spin-coated on pristine graphene (and with no thermal annealing) yielded DT signatures similar to those of region ①. This shows that PMMA physically deposited on graphene would not yield the signatures observed from region ②.

With the grafting of polymer molecules to graphene, two longer lived lifetimes are observed ($\tau''_2 = 390 \pm 50$ ps and $\tau''_3 >$ 1 ns − see Figure 4 inset) in addition to the short lifetime $\tau''_1 = 0.4 \pm 0.1$ ps (which is comparable to τ'_1 in region ① within experimental uncertainties). Given the laser spot size is ~5−10 μm, τ''_1 contains contributions from the pristine graphene as well. The similarities in τ'_1 and τ''_1 also implies that any initial trapping of the carriers to the localized states must have occurred in a time scale faster than or comparable to the electron−electron/electron−phonon relaxation processes.[27] Otherwise, the subsequent PL from the localized states would not be observed. τ''_2 is comparable with the short PL lifetime τ_1 while τ''_3 is comparable with the long PL lifetime τ_2, which correlates well with the above PL mechanism. These dynamical signatures are characteristic of the modulation of the electronic band structure from that of pristine graphene (i.e., with a Dirac cone) to one with a bandgap.[28,29]

Pump fluence dependent TA studies were also performed to gain a clearer understanding of the relaxation dynamics and mechanisms at these localized states. From Figure 5a, the
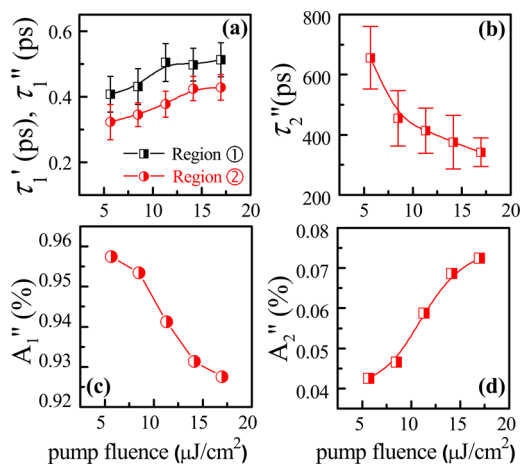
shorter lifetime increases with increasing pump fluence in both regions. In region ①, this increase in τ'_1 is attributed to the hot phonon bottleneck effect.[30,31] In region ②, the localized states will gradually be filled with increasing pump power. The state filling of these localized states will result in τ''_1 increasing and eventually becoming saturated. Do note that τ''_1 is always faster than τ'_1 for all pump fluence—consistent with our earlier interpretation of charge trapping to the localized states in region ②. The τ''_2 in region ② on the other hand decreases with increasing pump fluence—see Figure 5b. The weighting factor or pre-exponential factor A''_2 increases with pump fluence (see Figure 5c and d)—indicating an increasing contribution from τ''_2 at higher pump fluence. Such behavior is typical of an Auger type recombination[32,33] at the localized states.

Figure 6 shows the schematics of the carrier relaxation mechanisms in pristine graphene and in polymer-grafted

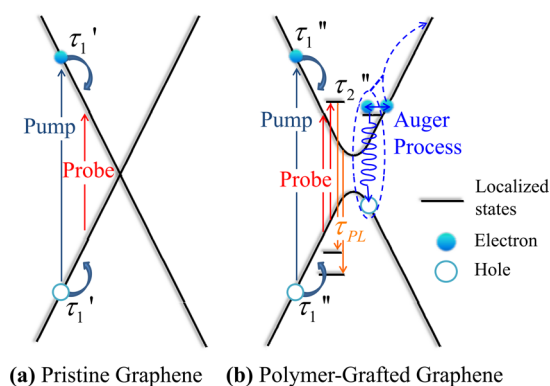**(a)** Pristine Graphene   **(b)** Polymer-Grafted Graphene

Figure 6. Schematics of the relaxation mechanisms in (a) pristine graphene and (b) polymer grafted graphene. Do note that the Auger recombination process at the localized states only occurs at high pump fluence.

graphene. In pristine graphene (Figure 6a) where there is no band gap, the excited carriers relax through electron−electron scattering (<10 fs) and electron−phonon scattering (i.e., with lifetime τ'_1) in the Dirac cone, without any photon emission. In the polymer-grafted graphene, the scenario is analogous to the cases of partially reduced GO[28,34] and intercalated graphene.[30,35] In addition to the opening of the bandgap, the grafted polymer molecules are also expected to introduce additional localized electronic states within the conduction and valence bands. The hot carriers relax through electron−electron scattering and electron−phonon scattering, and become trapped at these localized states within τ''_1 (see Figure 6b). These carriers in the localized states and the band edge eventually recombine to yield radiative emissions. At higher pump fluence, the hot phonon bottleneck and state filling effects become more dominant, leading to an increase of both τ'_1 and τ''_1. In addition, Auger effects at the localized states become more dominant as reflected by the decrease of τ''_2.

Figure 5. (a) Pump fluence dependence on the short lifetimes τ'_1 and τ''_1 from TAS. (b) Pump fluence dependence on the long lifetime τ''_2 from TAS. The corresponding pre-exponential factors or weighting factors in percentage from the fit of the pump-fluence dependent DT transients in Region ② are given in (c) and (d).

■ CONCLUSIONS

In conclusion, we have performed a comprehensive spatially resolved optical spectroscopy study to investigate the effects of grafted residual polymer molecules on the carrier dynamics in CVD graphene. Our findings revealed the occurrence of carrier trapping to localized states and the opening of a bandgap in graphene. Our work gives clear evidence of modulated fast electron−hole recombination dynamics in graphene by residual

polymer-grafted defects. Despite the negative connotations attached to such residues, this simple approach could potentially find practical use in tailoring the optoelectronic properties of graphene for light harvesting and spin manipulation.

■ ASSOCIATED CONTENT

Ⓢ Supporting Information

Details of spatially resolved transient absorption setup and results from the control experiments, Figure S1−S3. This material is available free of charge via the Internet at http://pubs.acs.org.

■ AUTHOR INFORMATION

Corresponding Author
*E-mail: tzechien@ntu.edu.sg.
Notes
The authors declare no competing financial interest.

■ ACKNOWLEDGMENTS

■ REFERENCES

(1) Novoselov, K. S.; Fal'ko, V. I.; Colombo, L.; Gellert, P. R.; Schwab, M. G.; Kim, K. A Roadmap for Graphene. *Nature* **2012**, *490* (7419), 192−200.

(2) Hwang, C.; Siegel, D. A.; Mo, S.-K.; Regan, W.; Ismach, A.; Zhang, Y.; Zettl, A.; Lanzara, A. Fermi velocity engineering in graphene by substrate modification. *Scientific Reports* **2012**, *2*, DOI: 10.1038/srep00590.

(3) Zhou, H.; Yu, W. J.; Liu, L.; Cheng, R.; Chen, Y.; Huang, X.; Liu, Y.; Wang, Y.; Huang, Y.; Duan, X. Chemical vapour deposition growth of large single crystals of monolayer and bilayer graphene. *Nature Communications* **2013**, *4*, DOI: 10.1038/ncomms3096.

(4) Li, X. L.; Wang, X. R.; Zhang, L.; Lee, S. W.; Dai, H. J. Chemically Derived, Ultrasmooth Graphene Nanoribbon Semiconductors. *Science* **2008**, *319* (5867), 1229−1232.

(5) Sun, Z. P.; Hasan, T.; Torrisi, F.; Popa, D.; Privitera, G.; Wang, F. Q.; Bonaccorso, F.; Basko, D. M.; Ferrari, A. C. Graphene Mode-Locked Ultrafast Laser. *ACS Nano* **2010**, *4* (2), 803−810.

(6) Dawlaty, J. M.; Shivaraman, S.; Chandrashekhar, M.; Rana, F.; Spencer, M. G. Measurement of Ultrafast Carrier Dynamics in Epitaxial Graphene. *Appl. Phys. Lett.* **2008**, *92* (4), 042116.

(7) Breusing, M.; Ropers, C.; Elsaesser, T. Ultrafast Carrier Dynamics in Graphite. *Phys. Rev. Lett.* **2009**, *102* (8), 086809.

(8) Huang, L.; Hartland, G. V.; Chu, L. Q.; Luxmi; Feenstra, R. M.; Lian, C.; Tahy, K.; Xing, H. Ultrafast Transient Absorption Microscopy Studies of Carrier Dynamics in Epitaxial Graphene. *Nano Lett.* **2010**, *10* (4), 1308−1313.

(9) Kumar, S.; Anija, M.; Kamaraju, N.; Vasu, K. S.; Subrahmanyam, K. S.; Sood, A. K.; Rao, C. N. R. Femtosecond Carrier Dynamics and Saturable Absorption in Graphene Suspensions. *App. Phys. Lett.* **2009**, *95* (19), 191911.

(10) Sun, D.; Wu, Z.-K.; Divin, C.; Li, X.; Berger, C.; de Heer, W.; First, P.; Norris, T. Ultrafast Relaxation of Excited Dirac Fermions in Epitaxial Graphene Using Optical Differential Transmission Spectroscopy. *Phys. Rev. Lett.* **2008**, *101* (15), 157402.

(11) Regan, W.; Alem, N.; Alemán, B. n.; Geng, B.; Girit, C. a. l.; Maserati, L.; Wang, F.; Crommie, M.; Zettl, A. A Direct Transfer of Layer-area Graphene. *Appl. Phys. Lett.* **2010**, *96* (11), 113102.

(12) Wu, W.; Yu, Q. K.; Peng, P.; Liu, Z. H.; Bao, J. M.; Pei, S. S. Control of Thickness Uniformity and Grain Size in Graphene Films for Transparent Conductive Electrodes. *Nanotechnol.* **2012**, *23* (3), 227−235.

(13) Lin, Y. C.; Lu, C. C.; Yeh, C. H.; Jin, C.; Suenaga, K.; Chiu, P. W. Graphene Annealing: How Clean Can it Be? *Nano Lett.* **2012**, *12* (1), 414−419.

(14) Terada, Y.; Yoshida, S.; Takeuchi, O.; Shigekawa, H. Real-Space Imaging of Transient Carrier Dynamics by Manoscale Pump-Probe Microscopy. *Nat. Photonics* **2010**, *4* (12), 869−874.

(15) Gao, B.; Hartland, G.; Fang, T.; Kelly, M.; Jena, D.; Xing, H. G.; Huang, L. Studies of Intrinsic Hot Phonon Dynamics in Suspended Graphene by Transient Absorption Microscopy. *Nano Lett.* **2011**, *11* (8), 3184−3189.

(16) Grancini, G.; Biasiucci, M.; Mastria, R.; Scotognella, F.; Tassone, F.; Polli, D.; Gigli, G.; Lanzani, G. Dynamic Microscopy Study of Ultrafast Charge Transfer in a Hybrid P3HT/Hyperbranched CdSe Nanoparticle Blend for Photovoltaics. *J. Phys. Chem. Lett.* **2012**, *3* (4), 517−523.

(17) Mehl, B. P.; Kirschbrown, J. R.; House, R. L.; Papanikolas, J. M. The End Is Different than The Middle: Spatially Dependent Dynamics in ZnO Rods Observed by Femtosecond Pump-Probe Microscopy. *J. Phys. Chem. Lett.* **2011**, *2* (14), 1777−1781.

(18) Sun, Z.; Yan, Z.; Yao, J.; Beitler, E.; Zhu, Y.; Tour, J. M. Growth of Graphene from Solid Carbon Sources. *Nature* **2010**, *468* (7323), 549−552.

(19) Xing, G. C.; Guo, H. C.; Zhang, X. H.; Sum, T. C.; Huan, C. H. A. The Physics of Ultrafast Saturable Absorption in Graphene. *Opt. Express* **2010**, *18* (5), 4564−4573.

(20) Diaz, J.; Paolicelli, G.; Ferrer, S.; Comin, F. Separation of the Sp(3) and Sp(2) Components in the C1s Photoemission Spectra of Amorphous Carbon Films. *Phys. Rev. B* **1996**, *54* (11), 8064−8069.

(21) Tomar, A. K.; Mahendia, S.; Chahal, R. P.; Kumar, S. Structural and Dielectric Spectroscopic Studies of Polyaniline-poly(methyl methacrylate) Composite Films. *Synth. Met.* **2012**, *162* (9−10), 820−826.

(22) Kudin, K. N.; Ozbas, B.; Schniepp, H. C.; Prud'homme, R. K.; Aksay, I. A.; Car, R. Raman Spectra of Graphite Oxide and Functionalized Graphene Sheets. *Nano Lett.* **2008**, *8* (1), 36−41.

(23) Zhang, Q.; Zheng, H. J.; Geng, Z. G.; Jiang, S. L.; Ge, J.; Fan, K. L.; Duan, S.; Chen, Y.; Wang, X. P.; Luo, Y. The Realistic Domain Structure of As-Synthesized Graphene Oxide from Ultrafast Spectroscopy. *J. Am. Chem. Soc.* **2013**, *135* (33), 12468−12474.

(24) Li, D.; Cutiongco, E.; Chung, Y. W.; Wong, M. S.; Sproul, W. D. Review of Synthesis and Characterization of Amorphous-Carbon Nitride Thin-Films. *Diamond Films Technol.* **1995**, *5* (5), 261−273.

(25) Lin, Y. C.; Lin, C. Y.; Chiu, P. W. Controllable Graphene N-doping with Ammonia Plasma. *App. Phys. Lett.* **2010**, *96* (13), 133110.

(26) Medina, H.; Lin, Y. C.; Obergfell, D.; Chiu, P. W. Tuning of Charge Densities in Graphene by Molecule Doping. *Adv. Funct. Mater.* **2011**, *21* (14), 2687−2692.

(27) Kaniyankandy, S.; Achary, S. N.; Rawalekar, S.; Ghosh, H. N. Ultrafast Relaxation Dynamics in Graphene Oxide: Evidence of Electron Trapping. *J. Phys. Chem. C* **2011**, *115* (39), 19110−19116.

(28) Shang, J. Z.; Ma, L.; Li, J. W.; Ai, W.; Yu, T.; Gurzadyan, G. G. The Origin of Fluorescence from Graphene Oxide. *Sci. Rep.* **2012**, *2*, 792 DOI: 10.1038/Srep00792.

(29) Eda, G.; Chhowalla, M. Chemically Derived Graphene Oxide: towards Large-Area Thin-Film Electronics and Optoelectronics. *Adv. Mater.* **2010**, *22* (22), 2392−415.

(30) Zou, X. Q.; Zhan, D.; Fan, X. F.; Lee, D.; Nair, S. K.; Sun, L.; Ni, Z. H.; Luo, Z. Q.; Liu, L.; Yu, T.; Shen, Z. X.; Chia, E. E. M. Ultrafast Carrier Dynamics in Pristine and FeCl₃-Intercalated Bilayer Graphene. *App. Phys. Lett.* **2010**, *97* (14), 141910.

(31) Betz, A. C.; Vialla, F.; Brunel, D.; Voisin, C.; Picher, M.; Cavanna, A.; Madouri, A.; Feve, G.; Berroir, J. M.; Placais, B.;

Pallecchi, E. Hot Electron Cooling by Acoustic Phonons in Graphene. *Phys. Rev. Lett.* **2012**, *109* (5), 056805.

(32) Rabani, E.; Baer, R. Theory of Multiexciton Generation in Semiconductor Nanocrystals. *Chem. Phys. Lett.* **2010**, *496* (4−6), 227−235.

(33) Rana, F. Electron-Hole Generation and Recombination Rates for Coulomb Scattering in Graphene. *Phys. Rev. B* **2007**, *76* (15), 155431.

(34) Liu, Z. B.; Zhao, X.; Zhang, X. L.; Yan, X. Q.; Wu, Y. P.; Chen, Y. S.; Tian, J. G. Ultrafast Dynamics and Nonlinear Optical Responses from sp(2)- and sp(3)-Hybridized Domains in Graphene Oxide. *J. Phys. Chem. Lett.* **2011**, *2* (16), 1972−1977.

(35) Zhan, D.; Sun, L.; Ni, Z. H.; Liu, L.; Fan, X. F.; Wang, Y. Y.; Yu, T.; Lam, Y. M.; Huang, W.; Shen, Z. X. FeCl3-Based Few-Layer Graphene Intercalation Compounds: Single Linear Dispersion Electronic Band Structure and Strong Charge Transfer Doping. *Adv. Funct. Mater.* **2010**, *20* (20), 3504−3509.